

Structure of the Bifunctional Acyltransferase/Decarboxylase LnmK from the Leinamycin Biosynthetic Pathway Revealing Novel Activity for a Double-Hot-Dog Fold

Jeremy R. Lohman,[†] Craig A. Bingman,^{||} George N. Phillips, Jr.,^{||,⊥} and Ben Shen^{*,†,‡,§}

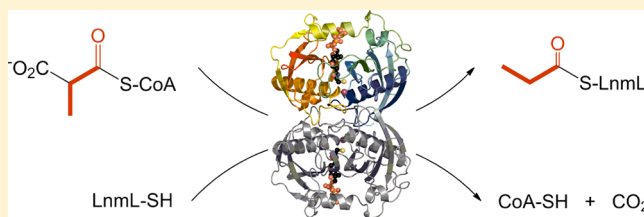
[†]Department of Chemistry, [‡]Department of Molecular Therapeutics, and [§]Natural Products Library Initiative at The Scripps Research Institute, The Scripps Research Institute, Jupiter, Florida 33485, United States

^{||}Department of Biochemistry, University of Wisconsin—Madison, Madison, Wisconsin 53706, United States

[⊥]Department of Biochemistry and Cell Biology, Rice University, Houston, Texas 77251, United States

S Supporting Information

ABSTRACT: The β -branched C3 unit in leinamycin biosynthesis is installed by a set of four proteins, LnmFKLM. In vitro biochemical investigation confirmed that LnmK is a bifunctional acyltransferase/decarboxylase (AT/DC) that catalyzes first self-acylation using methylmalonyl-CoA as a substrate and subsequently transacylation of the methylmalonyl group to the phosphopantetheinyl group of the LnmL acyl carrier protein [Liu, T., Huang, Y., and Shen, B. (2009) *J. Am. Chem. Soc.* 131, 6900–6901]. LnmK shows no sequence homology to proteins of known function, representing a new family of AT/DC enzymes. Here we report the X-ray structure of LnmK. LnmK is homodimer with each of the monomers adopting a double-hot-dog fold. Cocrystallization of LnmK with methylmalonyl-CoA revealed an active site tunnel terminated by residues from the dimer interface. In contrast to canonical AT and ketosynthase enzymes that employ Ser or Cys as an active site residue, none of these residues are found in the vicinity of the LnmK active site. Instead, three tyrosines were identified, one of which, Tyr62, was established, by site-directed mutagenesis, to be the most likely active site residue for the AT activity of LnmK. LnmK represents the first AT enzyme that employs a Tyr as an active site residue and the first member of the family of double-hot-dog fold enzymes that displays an AT activity known to date. The LnmK structure sets the stage for probing of the DC activity of LnmK through site-directed mutagenesis. These findings highlight natural product biosynthetic machinery as a rich source of novel enzyme activities, mechanisms, and structures.



Leinamycin (LNM), a potent antitumor antibiotic, is structurally characterized by an unusual 1,3-dioxo-1,2-dithiolane moiety that is spiro-fused to an 18-membered macrolactam ring of hybrid peptide–polyketide origin (Figure 1A).^{1–5} This molecular architecture has not been found in any other natural product to date. We have cloned, sequenced, and characterized the *lnm* biosynthetic gene cluster from *Streptomyces atroolivaceus* S-140.^{3–7} In vivo and in vitro characterizations of the LNM biosynthetic machinery unveiled that (i) the LNM backbone is assembled from the amino acid and short carboxylic acid precursors by a hybrid nonribosomal peptide synthetase (NRPS)-acyltransferase-less type I polyketide synthase (PKS)^{3–5} and (ii) the β -branched C3 unit, which is a part of the unique five-membered 1,3-dioxo-1,2-dithiolane moiety, is installed by a novel pathway for β -alkylation in polyketide biosynthesis (Figure 1A).^{8,9}

β -Alkylations contribute to the vast structural diversity displayed by polyketide natural products. The β -alkyl branches are installed by hydroxymethylglutaryl-CoA synthases (HCSs).^{9–16} HCS catalyzes condensation of an acyl-S-carrier protein (ACP) with the β -keto group of the growing ACP-tethered polyketide intermediate to afford a β -hydroxyacyl-S-

ACP intermediate. The latter undergoes further dehydration, decarboxylation, or both by one or both enoyl-CoA hydratases (ECH1 and ECH2) to afford a β -alkylated intermediate in polyketide biosynthesis (Figure 1A).

Two distinct pathways have been discovered for acyl-S-ACPs, i.e., acetyl-S-ACP and propionyl-S-ACP, the substrates of HCSs for β -alkylation in polyketide biosynthesis (Figure 1B).^{8–16} For acetyl-S-ACP, it is derived from malonyl-CoA by a dedicated set of three proteins, an ACP, an acyltransferase (AT), and a ketosynthase homologue (KS), and this pathway has been extensively studied in the biosynthesis of bacillaene, curacin, and myxovirescin (for the alkyl branch at C-12).^{10–16} For propionyl-S-ACP, it is derived from methylmalonyl-CoA by a dedicated set of two proteins, an ACP and a bifunctional acyltransferase/decarboxylase (AT/DC), and this pathway has been experimentally confirmed in the biosynthesis of LNM and predicted for the biosynthesis of myxovirescin (for the alkyl branch at C-16).⁸ Additional homologues of LnmK have also

Received: December 12, 2012

Revised: January 14, 2013

Published: January 15, 2013



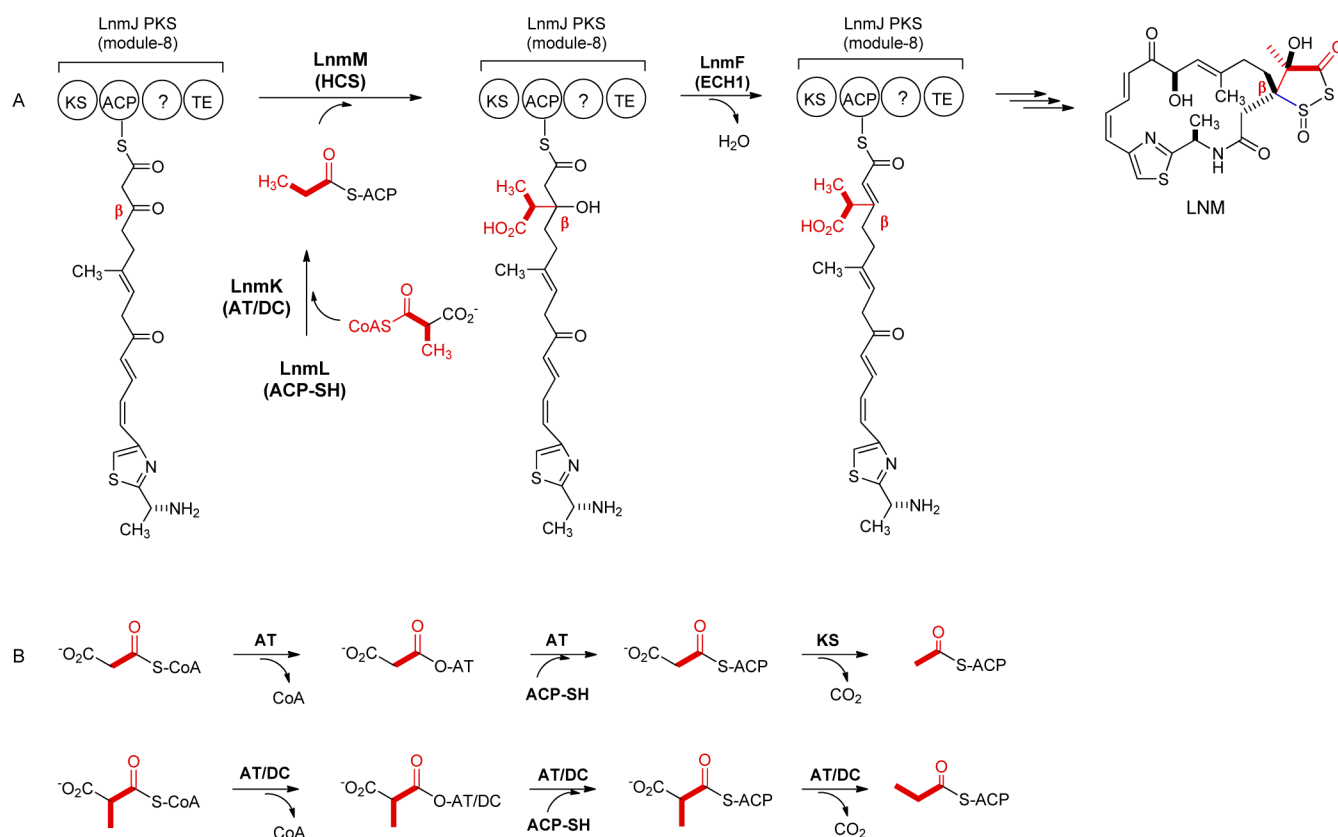


Figure 1. (A) Proposed LNM biosynthetic pathway featuring LnmKLM-catalyzed β -alkylation of the LnmJ PKS module 8 ACP-tethered intermediate in *S. atroolivaceus* S-140. (B) Two parallel but distinct pathways for the acyl-S-ACP substrate involved in β -alkylation in polyketide biosynthesis, i.e., acetyl-S-ACP from malonyl-CoA by dedicated ACP, AT, and KS enzymes and propionyl-S-ACP from methylmalonyl-CoA by a dedicated ACP and a bifunctional AT/DC enzyme.

been identified from recent genome sequencing efforts, all of which, however, were annotated as proteins of unknown function (Figure S1 of the Supporting Information).

Previously, we have demonstrated that the β -branched C3 unit in LNM biosynthesis is installed by a set of four proteins, LnmL, an ACP, LnmK, a bifunctional AT/DC, LnmM, a HCS, and LnmF, an ECH1.^{8,9} Inactivation of *lnmK*, *lnmL*, or *lnmM* in *S. atroolivaceus* S-140 abolished LNM production; the resultant mutant strains instead accumulated an identical set of shunt metabolites, all of which lack the β -branched C3 unit.⁹ In vitro biochemical investigation confirmed that LnmK is a bifunctional AT/DC: it is first self-acylated using methylmalonyl-CoA, the methylmalonyl group is then transferred from LnmK to the phosphopantetheinyl group of LnmL, and finally the resultant methylmalonyl-S-LnmL is decarboxylated to afford propionyl-S-LnmL (Figure 1B).⁸ LnmM-catalyzed condensation between propionyl-S-LnmL and the β -keto group of the growing polyketide intermediate, tethered to the ACP domain of LnmJ PKS module 8, followed by LnmF-catalyzed dehydration, completes the installation of the β -branch C3 unit into LNM (Figure 1A).⁹ While homologues of LnmF, LnmL, and LnmM are known, and their functions have been well characterized from several biosynthetic pathways of β -branched polyketides,^{10–16} LnmK shows no sequence homology to proteins of known function, representing a new family of AT/DC enzymes.^{8,9}

Here we report the X-ray structure of the bifunctional AT/DC enzyme LnmK. LnmK is a homodimer with each of the monomers adopting a double-hot-dog fold (DHDF). Cocrys-

tallization of LnmK with methylmalonyl-CoA revealed an active site tunnel terminated by residues from the dimer partner. In contrast to canonical AT and KS enzymes that employ Ser or Cys as an active site residue, none of these residues are found in the vicinity of the LnmK active site. Instead, three tyrosines were identified, one of which, Tyr62, was established, by site-directed mutagenesis, to be the most likely active site residue for the AT activity of LnmK. LnmK represents the first AT enzyme that employs a Tyr as an active site residue and the first identified member of the family of DHDF enzymes that displays an AT activity. The LnmK structure sets the stage for probing the DC activity of LnmK through site-directed mutagenesis. These findings highlight natural product biosynthetic machinery as a rich source of novel enzyme activities, mechanisms, and structures.

MATERIALS AND METHODS

Chemicals and Reagents. DL-2-[methyl-¹⁴C]Malonyl-CoA (American Radiolabeled Chemicals, St. Louis, MO), DL-methylmalonyl-CoA lithium salt (Sigma-Aldrich, St. Louis, MO), dNTPs (New England Biolabs, Ipswich, MA), and all other common biochemicals and chemicals were from standard commercial sources. Restriction enzymes and T4 DNA ligase (New England Biolabs), T4 DNA polymerase (Lucigen, Middleton, WI), and Platinum Pfx DNA polymerase (Invitrogen, Carlsbad, CA) were purchased. The pRSFDuet-1 plasmid and *Escherichia coli* NovaBlue and BL21(DE3) cells were from Novagen (Madison, WI). Primer synthesis and DNA

sequencing were performed at the University of Wisconsin—Madison Biotechnology Center (Madison, WI).

Plasmid Construction. To construct *lnmK* expression plasmid pBS3081, two oligos, TEV-1 F and TEV-1 R (see Table S1 of the Supporting Information), were annealed and ligated into the BamHI and XhoI sites of pRSFDuet-1 to afford pBS3080. The oligo insert contains a BsmFI site that allows for ligation-independent cloning and encodes a TEV protease site after the His₆ tag. pBS3080 was digested with BsmFI and purified by gel electrophoresis, and the linearized vector was treated with T4 DNA polymerase in the presence of dGTP at 20 °C for 30 min and then heated at 75 °C for 20 min to denature the polymerase, affording overhangs with complementary sequences to clone the PCR-amplified *lnmK* gene for expression. The *lnmK* gene was amplified by PCR from pBS3050⁸ using primers LnmK F and LnmK R (Table S1 of the Supporting Information), purified by gel electrophoresis, and similarly treated with T4 DNA polymerase in the presence of dCTP at 20 °C for 30 min and then heated at 75 °C. The T4 DNA polymerase-treated pBS3080 vector and *lnmK* fragment were then mixed at room temperature, annealed on ice for 5 min, and transformed into *E. coli* NovaBlue for ligation-independent cloning to construct *lnmK* expression plasmid pBS3081. pBS3081 was finally isolated from *E. coli* NovaBlue and confirmed by DNA sequencing, in which LnmK is produced as a fusion protein with an N-terminal His₆ tag that can be cleaved by TEV protease. Upon TEV cleavage, the resultant LnmK lacks the N-terminal methionine and contains a Thr2Ser mutation.

To construct *svp* and *lnmL* co-expression plasmid pBS3084, two oligos, TEV-2 F and TEV-2 R (Table S1 of the Supporting Information), were annealed and ligated into NcoI and BamHI sites of pRSFDuet-1 to afford pBS3082. The *svp* gene was amplified by PCR from pBS18¹⁷ with primers Svp F and Svp R (Table S1 of the Supporting Information) and ligated into the BglII site of pBS3082 to afford pBS3083, which was confirmed by DNA sequencing. The *lnmL* gene was amplified by PCR from pBS3051⁸ with primers LnmL F and LnmL R (Table S1 of the Supporting Information), and the resultant PCR product was digested and ligated into the BamHI and HindIII sites of pBS3083 to afford pBS3084, which was similarly confirmed by DNA sequencing. Co-expression of *svp* and *lnmL* in pBS3084 ensures the production of LnmL in its holo form, and LnmL is produced as a fusion protein with an N-terminal His₆ tag that can be cleaved by the TEV protease. Upon TEV cleavage, the resultant holo-LnmL lacks the N-terminal methionine and contains a Thr2Ser mutation.

Expression plasmids for the *lnmK* mutants (pBS3085–pBS3099) were constructed by following the QuicChange site-directed mutagenesis method (Stratagene, La Jolla, CA) with the primers summarized in Table S1 of the Supporting Information. Thus, the primer pairs for each of the *lnmK* mutant constructs were used to amplify *lnmK* from pBS3081. The resulting PCR products were digested with DpnI, purified by gel electrophoresis, and transformed into *E. coli* NovaBlue. The *lnmK* mutant constructs were isolated from *E. coli* NovaBlue, confirmed by DNA sequencing, and named pBS3085–pBS3097 (Table S1 of the Supporting Information). In these constructs, all LnmK mutants, i.e., Arg144Gln (pBS3085), Asn216Leu (pBS3086), Asn263Leu (pBS3087), Cys24Ala (pBS3088), Ser28Ala (pBS3089), Ser91Ala (pBS3090), Ser100Ala (pBS3091), Ser174Ala (pBS3092), Ser225Ala (pBS3093), Thr103Ala (pBS3094), Tyr62Phe

(pBS3095), Tyr222Phe (pBS3096), and Tyr226Phe (pBS3097), were produced as fusion proteins with an N-His₆ tag that can be cleaved by the TEV protease. Like LnmK from pBS3081, upon TEV cleavage, the resultant LnmK mutants all lack the N-terminal methionine and contain a Thr2Ser mutation.

Protein Production. Expression plasmids for *lnmL* (pBS3084), *lnmK* (pBS3081), and the *lnmK* mutants (pBS3085–pBS3097) were transformed into *E. coli* BL21- (DE3), and the resultant recombinant strains were grown overnight in 50 mL of LB containing 2 mM MgSO₄ and 50 µg/mL kanamycin. A 10 mL aliquot of the overnight culture was used to inoculate 1 L of LB containing 2 mM MgSO₄ and 50 µg/mL kanamycin, which was then incubated at 37 °C while being shaken at 250 rpm. Once the OD₆₀₀ reached ~0.4–0.5, the temperature was reduced to 18 °C. After the cultures had reached thermal equilibrium, gene expression was induced by the addition of isopropyl β-D-thiogalactopyranoside to a final concentration of 50 µg/mL, with incubation for an additional 16 h. For selenomethionine (Se-Met)-containing LnmK, *E. coli* BL21(DE3) was transformed with pBS3081 and incubated overnight in 50 mL of LB containing 2 mM MgSO₄ and 50 µg/mL kanamycin. A 5 mL aliquot of the overnight culture was introduced into autoinducing medium [50 mM Na₂HPO₄, 50 mM KH₂PO₄, 25 mM (NH₄)₂SO₄, 2 mM MgSO₄, 10 µM FeCl₃, 4 µM CaCl₂, 2 µM MnCl₂, 2 µM ZnSO₄, 0.4 µM CoCl₂, 0.4 µM CuCl₂, 0.4 µM NiCl₂, 0.4 µM Na₂MoO₄, 0.4 µM Na₂SeO₃, 0.4 µM H₃BO₃, 54 mM glycerol, 2.8 mM glucose, 5.6 mM lactose, Ala, Arg, Asn, Asp, Gln, Glu, Gly, His, Ile, Leu, Lys, Pro, Ser, Thr, Trp, Tyr, and Val (200 mg/L each), 10 mg/L Met, 125 mg/L Se-Met, and 100 nM vitamin B₁₂],¹⁸ containing 50 µg/mL kanamycin. The resultant culture was incubated at 37 °C while being shaken at 250 rpm for 4 h, at which time the temperature was reduced to 18 °C and incubation continued for 20 h. *E. coli* cells were harvested by centrifugation at 3500g and 4 °C for 20 min.

Protein Purification. *E. coli* cell pellets, carrying various expression constructs, were resuspended in lysis buffer [1 µg/mL DNase, 300 mM NaCl, 10 mM imidazole, 5% glycerol, and 50 mM Tris-HCl (pH 8.0)], sonicated (30 × 2 s on ice), and clarified by centrifugation at 50000g and 4 °C for 30 min. The supernatant was applied to a 5 mL Ni-Sepharose 6 Fast Flow column (GE Healthcare, Uppsala, Sweden) and washed with lysis buffer using an Äkta fast-performance liquid chromatography system (Pharmacia Amersham Biotech, Uppsala, Sweden). Wash buffer [300 mM NaCl, 20 mM imidazole, and 50 mM Tris-HCl (pH 8.0)] was used to remove additional contaminants, and proteins were eluted with wash buffer containing 250 mM imidazole. Proteins were immediately diluted from ~5 to 15 mL with buffer A [50 mM Tris-HCl (pH 8.0) and 10 mM NaCl] with 1 mM dithiothreitol, 0.1 mM EDTA, and 50 µg/mL TEV protease bearing a C-terminal His₆ tag and incubated overnight. The TEV-cleaved samples were further diluted to 50 mL with buffer A and passed over a Ni-Sepharose column to remove the TEV protease, and the flow through was then loaded onto a MonoQ 10/80 column (Pharmacia). A linear gradient over 12 column volumes from 10 to 50% buffer B [50 mM Tris-HCl (pH 8.0) and 1.0 M NaCl] was used to elute the proteins. The purity of the protein from the fractions was analyzed by sodium dodecyl sulfate–polyacrylamide gel electrophoresis (SDS–PAGE). Pure fractions were pooled, concentrated, buffer-exchanged into 10 mM Tris-HCl (pH 8.0) and 10 mM NaCl, frozen in small

aliquots with liquid nitrogen, and stored at -80°C . For the Ser, Thr, Cys, Arg, and Asn mutants of LnmK from pBS3085–pBS3097, the final step of MonoQ 10/80 column chromatography was omitted after the TEV protease removal step. Se-Met LnmK (from pBS3081) was not cleaved by TEV before MonoQ chromatography.

Size Exclusion Chromatography. LnmK was diluted to 1 absorbance unit at 280 nm ($\sim 25\ \mu\text{M}$) in 50 mM Tris-HCl (pH 8.0) and 50 mM NaCl, and 100 μL was loaded onto a Sepharose 6 10/300 GL column (GE lifesciences). A second sample with LnmK at 2 absorbance units ($\sim 50\ \mu\text{M}$) was mixed with 10 mM methylmalonyl-CoA and loaded onto the same column to examine the effect of methylmalonyl-CoA on the quaternary structure of LnmK. The column was eluted with 50 mM Tris-HCl (pH 8.0) and 50 mM NaCl at a flow rate of 1.0 mL/min and calibrated with molecular mass standards [thyroglobulin (660 kDa), ferritin (450 kDa), bovine serum albumin (66 kDa), and ribonuclease A (14 kDa)] (Figure S2 of the Supporting Information).

Enzymatic Assays of LnmK. LnmK-catalyzed loading of the methylmalonyl group from methylmalonyl-CoA to holo-LnmL, via a self-acylated intermediate, was assayed by following previously published procedures.⁸ A typical 50 μL self-acylation reaction mixture contained 100 mM Tris-HCl (pH 7.5), 10 mM MgCl_2 , 1 mM TCEP, and 20 μM DL-2-[methyl- ^{14}C]-malonyl-CoA, and the assay was initiated by the addition of 4 μM LnmK or one of the LnmK mutants. For transacylation, the same reaction mixtures were used but included additional 15 μM holo-LnmL. Reaction mixtures were incubated for varying amounts of time at 25°C and reactions quenched by the addition of 450 μL of acetone. Proteins were precipitated by centrifugation at 13000 rpm and 4°C for 10 min. Acetone was removed, and the pellet was allowed to air-dry for 10 min. The pellets were resuspended in sample buffer and subjected to SDS–PAGE on 4 to 15% gradient gels (Bio-Rad Laboratories, Hercules, CA). The gels were visualized by Coomassie blue staining and phosphorimaging (LE phosphor screen, Amersham Pharmacia, Molecular Dynamics Division, Piscataway, NJ).

Crystallization. LnmK was screened against 384 crystallization conditions in 200 nL sitting drops at 20°C , set up with a Mosquito (TTPlabtech, Melbourne, Australia) to find initial conditions. Se-Met LnmK [45 mg/mL in 10 mM NaCl and 10 mM Tris-HCl (pH 8.0)] and 2.5 mM methylmalonyl-CoA were screened by the hanging drop method over 0.5 mL wells containing 12–18% glycerol, 1.3–1.6 M $(\text{NH}_4)_2\text{SO}_4$, and 0.1 M Tris-HCl (pH 7.0–8.5) in 4 μL drops (1:1, protein:well), which produced crystals under all conditions. LnmK [20 mg/mL in 100 mM NaCl and 10 mM Tris-HCl (pH 8.0)] and 10 mM methylmalonyl-CoA were cocrystallized from 20–23% MEPEG 2000, 0.25–0.35 M $(\text{NH}_4)_2\text{SO}_4$, and 0.1 M Bis-tris propane-HCl (pH 7.0) in 4 μL drops (1:1, protein:well). LnmK (Tyr62Phe) was cocrystallized with methylmalonyl-CoA under conditions identical to those used for LnmK–methylmalonyl-CoA cocrystallization.

Data Collection, Phasing, Refinement, and Structural Determination. Crystals were frozen directly out of the drops with liquid nitrogen. X-ray diffraction data for Se-Met LnmK were collected at Advanced Photon Source LS-CAT Beamline 21-ID-D at a wavelength of 0.97941 Å for anomalous data sets and 1.127 Å for native sets. Beamline 21-ID-G at a wavelength of 0.97857 Å was used for LnmK–methylmalonyl-CoA and LnmK (Tyr62Phe)–methylmalonyl-CoA cocrystals. Diffraction

intensities were integrated, reduced, and scaled using HKL2000,¹⁹ and data collection and refinement statistics are listed in Table 1. Experimental phasing of the Se-Met LnmK

Table 1. Data Collection and Refinement Statistics

	Se-Met LnmK	LnmK–CoA	Tyr62Phe–CoA
Crystallographic Data			
space group	$P6_122$	$P6_122$	$P6_122$
cell dimensions	$a = b = 60.2\ \text{\AA}$, $c = 311.2\ \text{\AA}$ $\alpha = \beta = 90^{\circ}$, $\gamma = 120^{\circ}$	$a = b = 60.5\ \text{\AA}$, $c = 311.0\ \text{\AA}$ $\alpha = \beta = 90^{\circ}$, $\gamma = 120^{\circ}$	$a = b = 59.7\ \text{\AA}$, $c = 311.1\ \text{\AA}$ $\alpha = \beta = 90^{\circ}$, $\gamma = 120^{\circ}$
resolution (Å)	50.0–2.25	30.0–1.76	30.0–1.77
no. of observations	292008	323621	301960
no. of unique reflections	16907	34431	32885
completeness (%) ^a	98.8 (98.8)	97.7 (72.1)	98.5 (99.8)
$I/\sigma(I)$ ^a	28.7 (30.1)	16.0 (1.9)	14.7 (4.8)
R_{merge} (%) ^{a,b}	0.074 (0.105)	0.094 (0.673)	0.107 (0.570)
Refinement			
resolution (Å)	28.1–2.25	26.1–1.76	29.7–1.77
no. of reflections	15889	32402	30964
no. of protein atoms	2359	2388	2335
no. of waters	114	99	160
overall B factor (\AA^2)	23.1	34.7	27.4
protein B factor (\AA^2)	22.6	34.5	27.0
solvent B factor (\AA^2)	23.7	37.5	31.6
R factor ^c	0.202	0.219	0.227
R_{free}	0.254	0.249	0.275
rmsd for bonds (Å)	0.01	0.03	0.02
rmsd for angles (deg)	1.23	2.21	1.98
Ramachandran plot (%)			
most favored	92.3	90.7	90.6
allowed	7.7	9.3	9.4
disallowed	0	0	0

^aValues in parentheses indicate statistics for the highest-resolution shell. ^b $R_{\text{merge}} = \sum |I - \langle I \rangle| / \sum \langle I \rangle$, where I is the observed intensity and $\langle I \rangle$ is the average of intensities obtained from multiple observations of symmetry-related reflections. ^c R factor = $\sum ||F_o| - |F_c|| / \sum |F_o|$, where F_o and F_c are the observed and calculated structure amplitudes, respectively.

data set was performed using Phenix²⁰ against a number of space groups in the $P6_122$ point group. Refinement was conducted using Refmac²¹ in the CCP4i package²² with automated model building performed with ARP/wARP²³ and manual model building with Coot.²⁴ The refined structure of Se-Met LnmK served as the starting point for molecular replacement with cocrystal structures of LnmK and LnmK (Tyr62Phe) with methylmalonyl-CoA.

RESULTS

Crystallization and Structure Determination of LnmK.

Hanging drop experiments with Se-Met LnmK produced hexagonal crystals that appeared in 1 day and reached full size ($\sim 200\ \mu\text{m}$ in length) after ~ 4 days. Crystals diffracted

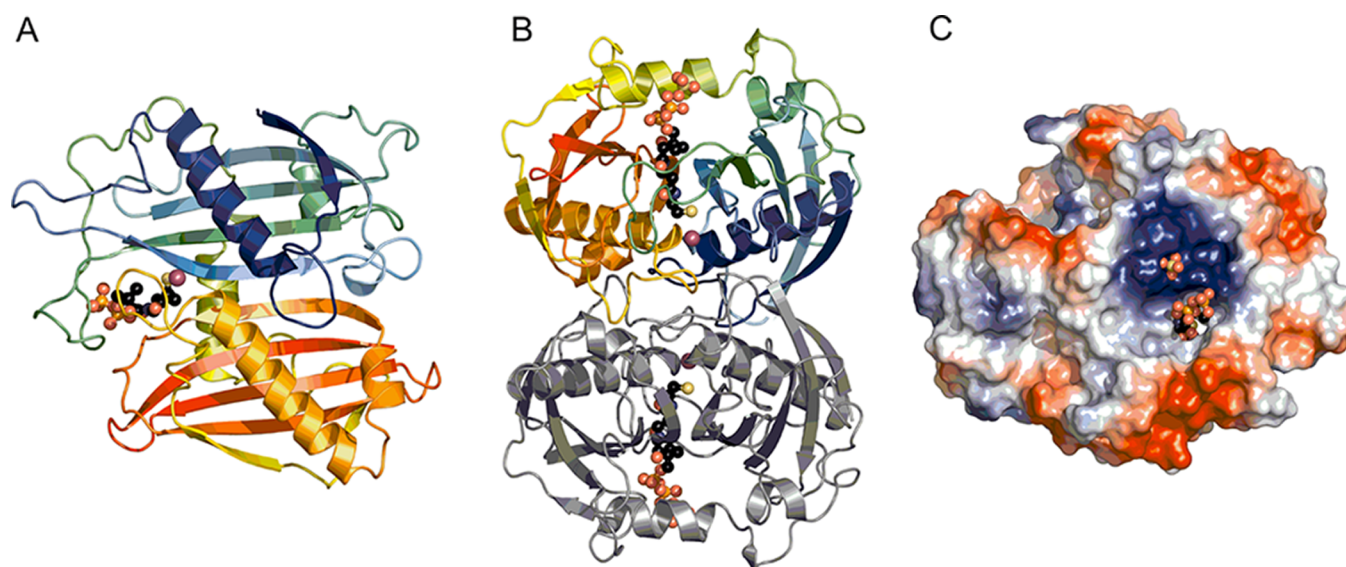


Figure 2. X-ray structure of LnmK. (A) Overall fold of LnmK, showing one monomer colored from the N-terminus (blue) to the C-terminus (red), the bound phosphopantetheine moiety as a black ball-and-stick model, and the bound chloride as a purple sphere. (B) Biologically relevant homodimer of LnmK with one monomer in color and one monomer in gray. (C) Electrostatic surface of LnmK revealing a basic patch surrounding the substrate binding tunnel to the active site with the phosphopantetheine moiety and a bound sulfate shown as a ball-and-stick model.

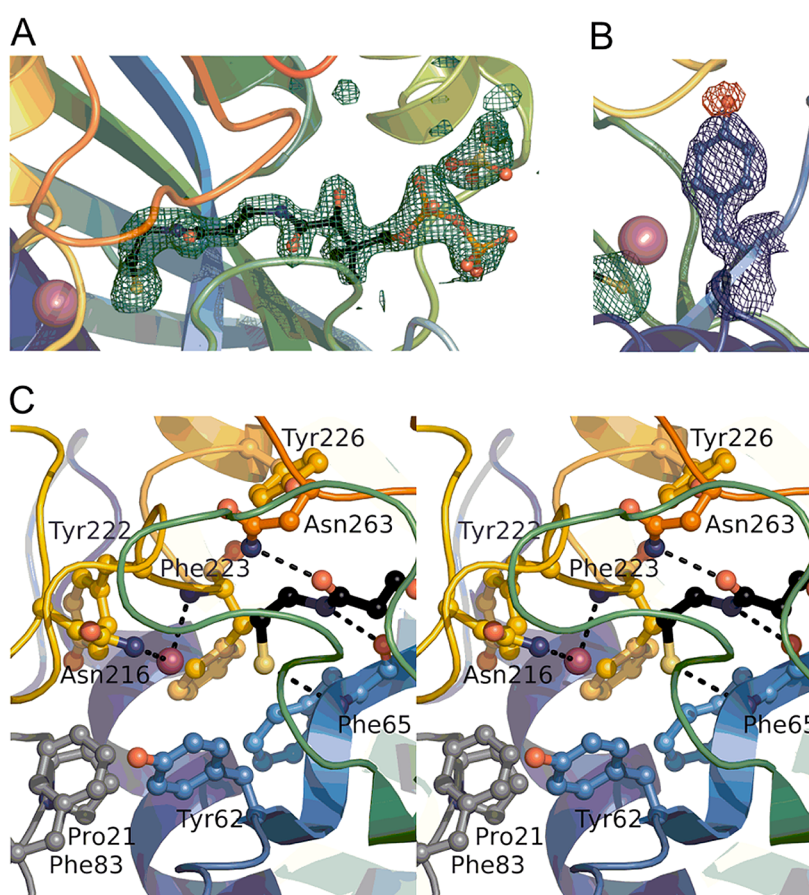


Figure 3. Active site of LnmK. (A) Sigma-weighted $F_o - F_c$ omit map at 3σ in green mesh depicting the phosphopantetheine moiety in the cocrystal structure of LnmK (Tyr62Phe) with methylmalonyl-CoA. (B) Tyrosine modeled into the cocrystal structure of LnmK (Tyr62Phe) with methylmalonyl-CoA showing the $2F_o - F_c$ map at 1σ colored blue and the $F_o - F_c$ map at -3σ colored red. (C) Stereoview showing the amino acid side chains lining the active site tunnel from the cocrystal structure of LnmK with methylmalonyl-CoA. The bound chloride is shown as a purple sphere. Residues emanating from the crystallographic dimer are colored gray.

maximally to ~ 1.7 Å in the hexagonal crystal system with the following cell dimensions: $a = b = 60.2$ Å, $c = 311.2$ Å, $\alpha = \beta =$

90° , and $\gamma = 120^\circ$. Because of the very long c cell dimension, very close spots were produced that overlapped at low

resolution and appropriate measures were taken to maximize data.²⁵ To obtain low-resolution data for phasing, a second data set was collected to only 2.25 Å. Scaling the high- and low-resolution data sets resulted in very large R_{merge} values; thus, higher-resolution data were omitted, and only the lower-resolution data set was used during phasing and refinement.

The $P6_122$ space group had the best phasing statistics and produced easily interpretable maps from Phenix AutoSol using the SAD data, indicating it was the correct space group (Table 1). Phenix AutoSol generated ~220 amino acids in five noncontinuous strands from the experimentally phased maps. The remainder of the structure was modeled using Coot. The final model consists of residues 11–309, 68 waters, five sulfates, one glycerol, and one Tris molecule. Despite the addition of 2.5 mM methylmalonyl-CoA to the crystallization drops, there is no clear electron density suggesting the presence of CoA or an acylated amino acid residue in the determined Se-Met LnmK structure. The final model refines to an R factor of 0.209 ($R_{\text{free}} = 0.270$). There are no residues in the disallowed region of the Ramachandran plot.

LnmK and LnmK (Tyr62Phe) were cocrystallized in the presence of methylmalonyl-CoA, which was hydrolyzed, resulting in LnmK–CoA and LnmK (Tyr62Phe)–CoA structures, which share the $P6_122$ space group. Molecular replacement was straightforward using the Se-Met LnmK structure after the removal of side chains and waters as a starting point for rigid body refinement. Both structures had reasonable data collection and refinement statistics (Table 1). The LnmK–CoA structure is very similar ($\text{rmsd} = 0.3$ Å) to the Se-Met LnmK structure except for the presence of the phosphopantetheine moiety of CoA and a chloride ion in the putative active site (Figures 2 and 3). The phosphopantetheine moiety had extra density hanging off the sulfur atom that could not be interpreted biologically and was left unmodeled. The LnmK (Tyr62Phe)–CoA structure has a phosphopantetheine moiety bound in the active site that lacks the extra density off the sulfur atom (Figure 3A) and clearly lacks the Tyr62 hydroxyl group (Figure 3B).

Overall Structure of LnmK. LnmK is a double “hot-dog fold” protein (DHDF) (Figure 2B).^{26,27} LnmK is comprised of 10 antiparallel β -sheet strands with a +2, +1, +1, –3, +5, +3, –1, –1, –2 topology. Residues 11–157 and 196–309 make up the N-terminal and C-terminal hot-dog folds (HDF), respectively (Figure 2A). Alignment of the individual HDFs produces a high degree of internal structural similarity ($\text{rmsd} = 2.3$ Å for 95 residues) yet only 7% internal sequence identity. The individual folds come together to create an extended β -sheet centered on a pseudo-two-fold axis. Residues 158–195 make up a loop extending the length of the protein with an intervening α -helix (residues 175–185, $\alpha 3$) that lies against the extended β -sheet opposite the side containing the wrapped α -helices. Basic residues emanating from $\alpha 3$ create a positively charged surface likely involved in electrostatic interactions with the negatively charged CoA and LnmL (Figure 2C). A tunnel through the protein is present between the individual HDFs, buttressed on one side by $\alpha 3$ and closed off on the opposite side by the C-terminal HDF α -helix and residues emanating from other loops. The hole is blocked on one side by a symmetry mate that forms the active site cavity (Figure 2). The large surface area buried between the crystallographic monomer and symmetry mate is indicative of dimerization of LnmK (1745 Å², PISA calculated²⁸), which was confirmed by size exclusion chromatography. LnmK (calculated molecular mass

of 35 kDa) was eluted as a homodimer with an apparent molecular mass of 66 kDa, and addition of methylmalonyl-CoA had no effect on the quaternary structure of LnmK (Figure 4 and Figure S2 of the Supporting Information).

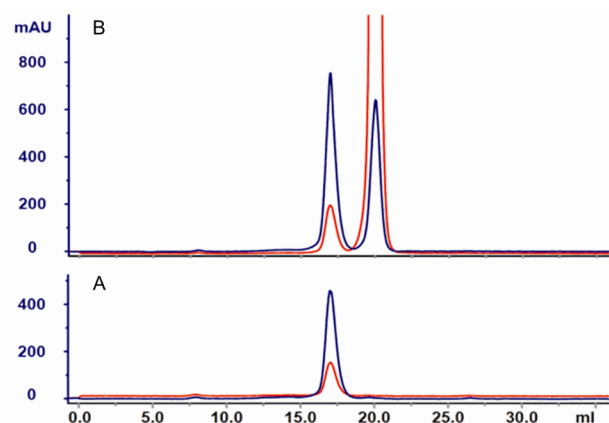


Figure 4. Quaternary structure of LnmK as a homodimer determined by size exclusion chromatography of LnmK at (A) 1 absorbance unit and (B) 2 absorbance units at 280 nm with 10 mM methylmalonyl-CoA with UV detection at 260 nm (red) and 280 nm (blue).

Comparison of LnmK by a structural similarity search of the Protein Data Bank (PDB) with Dali²⁹ revealed homology to a variety of enzymes with acyl-CoA or acyl-ACP thioesterase, dehydratase, and isomerase activities, but none with confirmed acyltransferase activity. Very few structural homologues have >15% identity at the primary sequence level, with the highest being 21% for a *Pseudomonas aeruginosa* hypothetical protein (unpublished PDB entry 1SH8, $\text{rmsd} = 7.9$ Å) comprised of a single HDF. One of the most structurally similar proteins is acyl-CoA thioesterase 12 (hTE12, unpublished PDB entry 3B7K, 12% sequence identity, $\text{rmsd} = 3.9$ Å), and the alignment reveals a similar binding of CoA against $\alpha 3$ (Figure S3 of the Supporting Information).

AT Active Site of LnmK. Although LnmK and the LnmK (Tyr62Phe) mutant were cocrystallized with methylmalonyl-CoA, density in the active site tunnel clearly represents the CoA hydrolysis product (Figure 3). Hydrolysis of the substrate is a known side reaction for malonyl-CoA:ACP acetyltransferases⁴ and explains the similar activity for LnmK. Electron density for the adenosine portion of methylmalonyl-CoA is also lacking, likely because of a combination of hydrolysis and conformational heterogeneity. In the LnmK (Tyr62Phe)–CoA structure, a sulfate ion is bound near the phosphate moiety of the phosphopantetheine moiety and is sufficiently close in space to represent the ribose phosphate, even though there is no clear density for the sugar moiety (Figure 3A). The clear density for the phosphopantetheine moiety in the structure points to an active site, with the phosphate group exposed to solvent and the thiol group buried in the core of the protein (Figures 2 and 3). A tunnel through the enzyme surrounds the phosphopantetheine moiety, which is lined by main chain atoms and hydrophobic residues (Val142, Ala64, Leu221, Gly262, Leu153, Leu261, and Tyr66) (Figure 5). The phosphopantetheine moiety interacts with the tunnel via a few specific hydrogen bonds: the Asn263 side chain bonds with the β -alanine carbonyl moiety, the backbone carbonyl of Tyr260 bonds with the β -alanine amide, the carbonyl of Phe65 bonds with the cysteamine moiety amide, the Leu153 amide

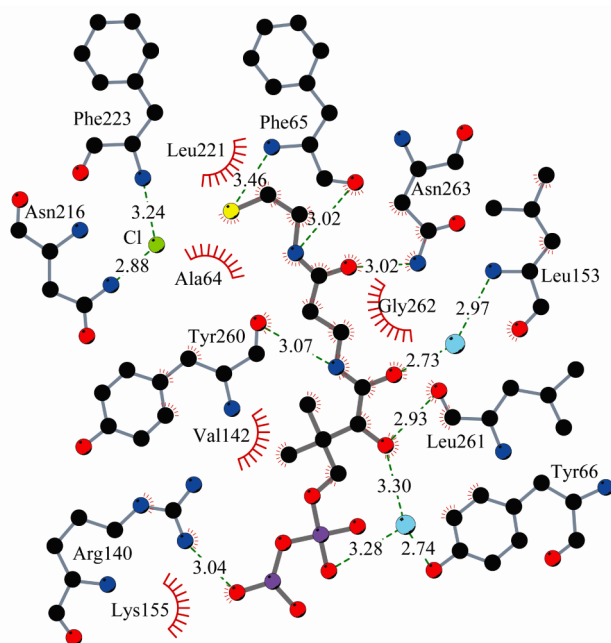


Figure 5. Flattened map of the LnmK active site tunnel showing key interactions between the bound phosphopantetheine moiety and the amino acid residues lining the active site tunnel.

interacts with the pantoate carbonyl via a water, the pantoate hydroxyl moiety is bonded to the Leu261 carbonyl and to the Tyr66 hydroxyl via a water molecule, and the terminal thiol is 3.5 Å from the amide of Phe65 (Figure 5). Phe83 and Pro21 from the symmetry mate form a plug at one end of the tunnel forming an active site cavity (Figure 3C). A chloride ion is bound in the base of the active site by the backbone carbonyl of Phe223 and Asn216 (Figure 3C). There are no serine, threonine, or cysteine residues in the cavity to act as a nucleophile for accepting and donating the methylmalonyl unit, as would be predicted from acyltransferases known to date. However, there are three tyrosines (Tyr62, Tyr222, and Tyr226) bearing the hydroxyl groups, serving as alternative but unprecedented candidates for the active site residue of an AT (Figure 3C).

Comparison of the Se-Met and native LnmK structures reveals conformational changes for two tyrosines at the entrance of the active site tunnel upon CoA–LnmL binding.

In the Se-Met structure, Tyr66 blocks the active site tunnel entrance, and upon rotation away from the tunnel, it would clash with Tyr179, which must move in response. The latter is exactly what was observed in the cocrystal structures of LnmK and LnmK (Tyr62Phe) with methylmalonyl-CoA (Figure S4 of the Supporting Information). Also observed in the Se-Met LnmK structure is one primary hydroxyl of a glycerol molecule bound in the tunnel in a position similar to that of the sulfur in the cocrystal structures of LnmK and LnmK (Tyr62Phe) with methylmalonyl-CoA (Figure S5 of the Supporting Information), and this may explain why the phosphopantetheine moiety is not bound in the Se-Met LnmK structure. One of the bound solvent sulfate ions is found around the basic surface near the entrance to the active site tunnel.

Testing the AT Active Site Residues of LnmK. To test the hypothesis that LnmK employs a tyrosine as the catalytic nucleophile, Tyr62, Tyr222, and Tyr226 were mutated to phenylalanine (Figure 3C) and tested using DL-2-[methyl-¹⁴C]-malonyl-CoA as a substrate (Figure 1B). LnmK Tyr222Phe and Tyr226Phe mutants behaved as the native enzyme, but Tyr62Phe lost both self-acylation (Figure 6A) and transacylation activities (Figure 6B,C), implicating Tyr62 as the active site residue with its hydroxyl group acting as the catalytic nucleophile (Figure 6). Asn216 and Asn263 were mutated to leucine, which reduced AT activity (lanes 5 and 6 of Figure S6 of the Supporting Information), and this finding is consistent with their predicted roles in anchoring the CoA–LnmL complex within the active site tunnel (Figure 3C). All conserved Ser, Thr, and Cys residues among LnmK and homologues were identified (Figure S1 of the Supporting Information) and mutated to interrogate their function in AT catalysis. The Cys24Ala, Ser28Ala, Ser100Ala, Thr130Ala, Ser174Ala, and Ser225Ala mutants all retained activity (Figure S6 of the Supporting Information), and the diminished activity of the Ser91Ala mutant resulted from its thermo-instability (lane 12 of Figure S6 of the Supporting Information). The Ser91Ala mutant precipitated when the assay solution was heated to 25 °C, and this is consistent with the observation that Ser91 is buried and makes important contacts for LnmK structural integrity. Taken together, these results point to Tyr62 as the active site residue, the hydroxy group of which acts as the nucleophile and forms an acyl-O-Tyr intermediate in AT catalysis (Figure 1B). Similar to known acyltransferases that employ Ser at their active sites, LnmK also hydrolyzes substrate methylmalonyl-CoA (Figure 6A) and product propionyl-S-

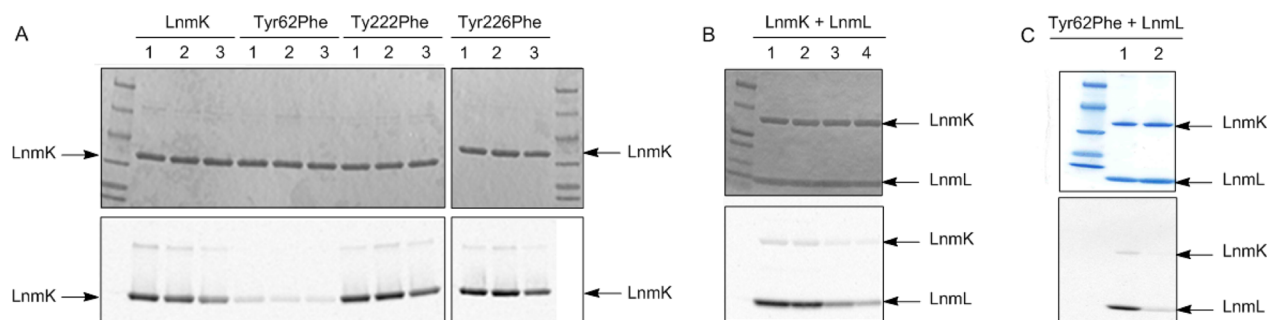


Figure 6. Enzymatic assays and time courses of LnmK and the LnmK Tyr62Phe, Tyr222Phe, and Tyr226Phe mutants for their AT activity with DL-2-[methyl-¹⁴C]malonyl-CoA as a substrate upon SDS–PAGE (4 to 15%) (top) and autoradiography (bottom) analyses. (A) Self-acylation of LnmK in comparison to the three Tyr62Phe, Tyr222Phe, and Tyr226Phe mutants with varying incubation times (lane 1, 10 s; lane 2, 140 s; lane 3, 1000 s). (B) Transacylation to LnmL by LnmK with varying incubation times (lane 1, 0.5 min; lane 2, 5 min; lane 3, 20 min; lane 4, 60 min). (C) Transacylation to LnmL by LnmK in comparison with the Tyr62Phe mutant with a 1 min incubation time.

LnmL (Figure 6B) over extended incubations, which is likely the reason for the absence of methylmalonyl-CoA or an acylated residue in the active site of the crystal structures of LnmK.

DISCUSSION

LnmK Representing a New Family of AT/DC Enzymes.

β -Alkyl branches in polyketide biosynthesis are installed by HCSs, which utilize acetyl-S-ACP and propionyl-S-ACP to furnish the β -methyl and β -ethyl/propionyl branches, respectively.^{9–16} Two parallel but distinct pathways have been discovered for acetyl-S-ACP and propionyl-S-ACP biosynthesis (Figure 1B). Acetyl-S-ACP from malonyl-CoA is catalyzed by a dedicated set of ACP, AT, and KS (acting as a DC). This pathway has been characterized from several types of polyketide biosynthetic machinery, and both the AT and KS enzymes show a high degree of sequence homology to proteins of known AT and KS activities.^{8–16} Propionyl-S-ACP from methylmalonyl-CoA by a dedicated ACP (LnmL) and a bifunctional AT/DC (LnmK) was first reported for the LNM biosynthetic machinery (Figure 1A).⁸ Although the AT activity and DC activity of LnmK were established biochemically (Figure 1B)⁸ and homologues of LnmK have been identified from other biosynthetic pathways (Figure S1 of the Supporting Information), LnmK shows no sequence homology to either ATs or DCs known to date, representing a new family of bifunctional AT/DC enzymes.

We now report the X-ray crystal structures of LnmK at 1.7 Å resolution (Table 1). LnmK is a homodimer composed of two monomeric DHDFs (Figure 2). Each monomer possesses an active site tunnel terminated by residues emanating from the dimer partner, which is revealed through cocrystallization with the substrate methylmalonyl-CoA (Figure 3). The crystal structures set the stage for exploring the utility of LnmK in engineering polyketide structural diversity by providing a molecular surface to interrogate the interaction with LnmL and by revealing the putative active site residues to determine LnmL-tethered substrate specificity. Most importantly, these structures reveal surprising deviations from the known chemical mechanisms of either AT and KS enzymes or DHDF enzymes. LnmK represents the first AT that employs a Tyr as an active site residue and the first member of the family of DHDF enzymes that displays an AT activity (Figures 3C and 6). These findings highlight natural product biosynthetic machinery as a rich source of novel enzyme activities, mechanisms, and structures. Mechanistic and structural characterization of novel enzymes for natural product biosynthesis will greatly facilitate efforts to engineer natural product structural diversity for drug discovery and development by combinatorial biosynthesis strategies.

A New Member of the HDF Family. Members of the HDF family often share little sequence homology but can be structurally similar; this leads to a large number of functions within this structure family.^{26,27} Nevertheless, AT activity has not been demonstrated by a HDF enzyme to date. The majority of HDFs are acyl-CoA thioesterases and dehydratases involved in primary metabolism. Recently, the activities of this family have grown from the characterizations of natural product biosynthetic machinery, including dehydratase domains with DHDFs from erythromycin (PDB entry 3EL6)³⁰ and curacin (PDB entries 3KG6, 3KG7, 3KG8, and 3KG9),³¹ type I polyketide synthases, the product template domains with DHDFs from fungal type I polyketide synthase (PDB entries

3HRR and 3HRQ),^{32,33} and thioesterases with HDFs from enediyne biosynthetic machinery (PDB entries 2XFL, 2XEM, and 2W3X).^{34–36} LnmK shares a similar overall fold with these enzymes associated with natural product biosynthesis, yet their structures are quite different, with rmsd values in the range of 4.4–4.9 Å for the DHDF enzymes and 2–3.2 Å for the single-HDF enzymes (Figure S7 of the Supporting Information). The active site entrance of LnmK is located at the meeting point between the individual HDFs (Figure 2), while the active site entrance of the product template domain and dehydratases is located within one of the HDFs (Figure S7 of the Supporting Information). LnmK is structurally more similar to the DHDF acyl-CoA and acyl-ACP thioesterases and dehydratases from primary metabolism with respect to the location of the active site (Figure S7 of the Supporting Information). The dehydratases utilize conserved Asp and His in the active sites for activity, and the DHDF thioesterases use a variety of mechanisms for catalysis, including an Asp, Thr, and Gln catalytic triad to activate a water molecule for nucleophilic attack, or direct attack of an Asp or Glu on a thioester activated by backbone amides.^{26,27} LnmK lacks these typical catalytic residues in the active site, making the enzymatic mechanism enigmatic (Figure 3). Although LnmK is structurally very similar to hTE12, an acyl-CoA thioesterase, the binding modes of CoA are very different; whereas the interactions of LnmK with CoA are mainly through the phosphopantetheine moiety and electrostatic interactions with the ribose phosphate, hTE12 binds the adenine moiety (Figure S3 of the Supporting Information). These comparisons serve to highlight the unique structure of LnmK as a DHDF family member that catalyzes unprecedented AT/DC activity and the versatility of this unique structural fold in acquiring and evolving new enzymatic activity.

An AT Mechanism Based on Tyrosine. Canonical (methyl)malonyl-CoA:ACP acyltransferases use a Ser as the catalytic nucleophile.^{37–40} The active site of these ATs is rigid in nature with all the catalytic residues set in place, such that conformational changes during catalysis are minimal.^{37–40} The cocrystal structures of LnmK and LnmK (Tyr62Phe) with methylmalonyl-CoA reveal no Ser in the vicinity of the active site but instead three tyrosines (Tyr62, Tyr222, and Tyr226) as alternative active site residues of an AT (Figure 3C). Site-directed mutagenesis indeed confirmed that Tyr62 is the most likely residue to act as the catalytic nucleophile; the LnmK (Tyr62Phe) mutant completely loses its AT activities in both self-acylation (Figure 6A) and transacylation to LnmL (Figure 6B,C), whereas the LnmK (Tyr222Phe) and LnmK (Tyr226Phe) mutants retain the same activity as the native LnmK (Figure 6). The crystal structure of LnmK (Tyr62Phe) confirms that the mutant is still properly folded and should be catalytically competent if the Tyr62 hydroxyl was not necessary for activity. Unfortunately, LnmK (Tyr62Phe) still hydrolyzed methylmalonyl-CoA, which otherwise would have revealed the binding interactions of the methylmalonyl moiety. In all of the structures, the Tyr62 hydroxyl faces away from the active site, such that there would have to be rotation about the $\text{C}\alpha\text{--C}\beta$ bond to bring the hydroxyl near the bound thioester (Figure 3C). Evidence of such a conformational change is suggested by a distorted β -sheet bulge between Tyr62 and Leu63 that upon relaxation could drive the repositioning of Tyr62 into the active site. This needed conformational change masks the identity of the catalytic base responsible for activation of the tyrosine. Together, the use of a tyrosine as

the catalytic nucleophile and the need for conformational changes make the AT mechanism of LnmK unique. These findings are sure to inspire and inform the search for ATs and other natural product biosynthetic machinery that employ noncanonical active sites.

AT and DC Activity from the Same Active Site. The decarboxylation reaction most likely takes place within the phosphopantetheine binding site, as the only pockets of conserved residues lie in this active site and dimerization interface (Figure S1 of the Supporting Information). There are various ways enzymes catalyze the decarboxylation of β -keto acids. Minimally, these enzymes must maintain a deprotonated carboxylate, align electron orbital overlap, and stabilize the enolate intermediate. The well-studied acetoacetate decarboxylase uses a lysine to form an enamine with the ketone group that stabilizes the intermediate enolate and an arginine to maintain a deprotonated carboxylate.⁴¹ Methylmalonyl-CoA decarboxylase is proposed to use two backbone amides to stabilize the thioester enolate oxygen, while a nearby histidine likely protonates the α -carbon.⁴² KSs utilize a conserved histidine to stabilize the thioester enolate oxygen.^{43–45} The lack of acids and bases in the active site of LnmK makes it difficult to propose a mechanism. Nevertheless, in the cocrystal structures of LnmK and LnmK (Tyr62Phe) with methylmalonyl-CoA, a chloride is bound between the backbone amide of Phe223 and the side chain of Asn216, which may be analogous to the carbonyl binding mode in methylmalonyl-CoA decarboxylase (Figure 3). The LnmK structure will allow us to probe the DC reaction through targeted mutagenesis of the active site residues and analysis of the resulting acyl group carried by LnmL, to understand the complex chemistry conducted by this novel bifunctional AT/DC enzyme.

■ ASSOCIATED CONTENT

■ Supporting Information

Oligos and primers used (Table S1), LnmK and its homologues and conservation scores painted on the LnmK structure (Figure S1), calibration with molecular mass standards for size exclusion chromatography of LnmK on a Sepharose 6 10/300 GL column (Figure S2), structural alignment of LnmK with hTE12 (Figure S3), conformational change upon substrate binding as revealed by comparison between the structures of Se-Met LnmK, LnmK, and LnmK (Tyr62Phe) in complex with phosphopantetheine (Figure S4), structure of Se-Met LnmK with glycerol bound at the active site tunnel as compared with the structures of LnmK and LnmK (Tyr62Phe) in complex with CoA (Figure S5), enzymatic assays of LnmK and selected mutants examining their AT activity in transacylation to LnmL with DL-2-[methyl-¹⁴C]malonyl-CoA as a substrate upon SDS-PAGE and autoradiography analyses (Figure S6), and selected enzymes characterized from natural product biosynthetic machinery that adopt a HDF (Figure S7). This material is available free of charge via the Internet at <http://pubs.acs.org>.

Accession Codes

The atomic coordinates and structure factors of Se-Met LnmK, LnmK, and LnmK (Tyr62Phe) in complex with CoA have been deposited as PDB entries 4HZN, 4HZO, and 4HZP, respectively.

■ AUTHOR INFORMATION

Corresponding Author

*The Scripps Research Institute, 130 Scripps Way, #3A1, Jupiter, FL 33458. Telephone: (561) 228-2456. Fax: (561) 228-2472. E-mail: shenb@scripps.edu.

Funding

This work was supported in part by National Institute of General Medical Sciences Protein Structure Initiative Grant GM094596 (G.N.P. and B.S.) and National Institutes of Health Grant CA106150 (B.S.).

Notes

The authors declare no competing financial interests.

■ ACKNOWLEDGMENTS

We thank Kyowa Hakko Kogyo Co. Ltd. (Tokyo, Japan) for the wild-type *S. atroolivaceus* S-140 strain and the Advanced Photon Source LS-CAT beamline staff, especially David Smith, for assistance with X-ray data collection. Use of the Advanced Photon Source was supported by the U.S. Department of Energy, Office of Science, Office of Basic Energy Sciences (Contract DE-AC02-06CH11357), and use of LS-CAT Sector 21 was supported by the Michigan Economic Development Corp. and the Michigan Technology Tri-Corridor (Grant 08SP1000817).

■ ABBREVIATIONS

ACP, acyl carrier protein; AT, acyltransferase; DC, decarboxylase; ECH, enoyl-CoA hydratase; HCS, hydroxymethylglutaryl-CoA synthase; KS, ketosynthase; LNM, leinamycin; NRPS, nonribosomal peptide synthetase; PCR, polymerase chain reaction; PKS, polyketide synthase; rmsd, root-mean-square deviation; Se-Met, selenomethionine.

■ REFERENCES

- (1) Hara, M., Asano, K., Kawamoto, I., Takiguchi, T., Katsumata, S., Takahashi, K., and Nakano, H. (1989) Leinamycin, a new antitumor antibiotic from *Streptomyces*: Producing organism, fermentation and isolation. *J. Antibiot.* 42, 1768–1774.
- (2) Hirayama, N., and Matsuzawa, E. S. (1993) Molecular structure of a novel antitumor antibiotic leinamycin. *Chem. Lett.*, 1957–1958.
- (3) Cheng, Y.-Q., Tang, G.-L., and Shen, B. (2002) Identification and localization of the gene cluster encoding biosynthesis of the antitumor macrolactam leinamycin in *Streptomyces atroolivaceus* S-140. *J. Bacteriol.* 184, 7013–7024.
- (4) Cheng, Y., Tang, G., and Shen, B. (2003) Type I polyketide synthase requiring a discrete acyltransferase for polyketide biosynthesis. *Proc. Natl. Acad. Sci. U.S.A.* 100, 3149–3154.
- (5) Tang, G., Cheng, Y., and Shen, B. (2004) Leinamycin biosynthesis revealing unprecedented architectural complexity for a hybrid polyketide synthase and nonribosomal peptide synthetase. *Chem. Biol.* 11, 33–45.
- (6) Tang, G., Cheng, Y., and Shen, B. (2006) Polyketide chain skipping mechanism in the biosynthesis of the hybrid nonribosomal peptide-polyketide antitumor antibiotic leinamycin in *Streptomyces atroolivaceus* S-140. *J. Nat. Prod.* 69, 387–393.
- (7) Tang, G.-L., Cheng, Y.-Q., and Shen, B. (2007) Chain initiation in the leinamycin-producing hybrid nonribosomal peptide/polyketide synthetase from *Streptomyces atroolivaceus* S-140. Discrete, monofunctional adenylation enzyme and peptidyl carrier protein that directly load D-alanine. *J. Biol. Chem.* 282, 20273–20282.
- (8) Liu, T., Huang, Y., and Shen, B. (2009) Bifunctional acyltransferase/decarboxylase LnmK as the missing link for β -alkylation in polyketide biosynthesis. *J. Am. Chem. Soc.* 131, 6900–6901.

- (9) Huang, Y., Huang, S.-X., Ju, J., Tang, G., Liu, T., and Shen, B. (2011) Characterization of the *ImmKLM* genes unveiling key intermediates for β -alkylation in leinamycin biosynthesis. *Org. Lett.* 13, 498–501.
- (10) Calderone, C. T., Kowtoniuk, W. E., Kelleher, N. L., Walsh, C. T., and Dorrestein, P. C. (2006) Convergence of isoprene and polyketide biosynthetic machinery: Isoprenyl-S-carrier proteins in the pksX pathway of *Bacillus subtilis*. *Proc. Natl. Acad. Sci. U.S.A.* 103, 8977–8982.
- (11) Gu, L., Jia, J., Liu, H., Håkansson, K., Gerwick, W. H., and Sherman, D. H. (2006) Metabolic coupling of dehydration and decarboxylation in the curacin A pathway: Functional identification of a mechanistically diverse enzyme pair. *J. Am. Chem. Soc.* 128, 9014–9015.
- (12) Simunovic, V., Zapp, J., Rachid, S., Krug, D., Meiser, P., and Müller, R. (2006) Myxovirescin A biosynthesis is directed by hybrid polyketide synthases/nonribosomal peptide synthetase, 3-hydroxy-3-methylglutaryl-CoA synthases, and trans-acting acyltransferases. *ChemBioChem* 7, 1206–1220.
- (13) Calderone, C. T., Iwig, D. F., Dorrestein, P. C., Kelleher, N. L., and Walsh, C. T. (2007) Incorporation of nonmethyl branches by isoprenoid-like logic: Multiple β -alkylation events in the biosynthesis of myxovirescin A1. *Chem. Biol.* 14, 835–846.
- (14) Simunovic, V., and Müller, R. (2007) 3-Hydroxy-3-methylglutaryl-CoA-like synthases direct the formation of methyl and ethyl side groups in the biosynthesis of the antibiotic myxovirescin A. *ChemBioChem* 8, 497–500.
- (15) Calderone, C. T. (2008) Isoprenoid-like alkylations in polyketide biosynthesis. *Nat. Prod. Rep.* 25, 845–853.
- (16) Buchholz, T. J., Rath, C. M., Lopanik, N. B., Gardner, N. P., Håkansson, K., and Sherman, D. H. (2010) Polyketide β -branching in bryostatin biosynthesis: Identification of surrogate acetyl-ACP donors for BryR, an HMG-ACP synthase. *Chem. Biol.* 17, 1092–1100.
- (17) Sánchez, C., Du, L., Edwards, D. J., Toney, M. D., and Shen, B. (2001) Cloning and characterization of a phosphopantetheinyl transferase from *Streptomyces verticillus* ATCC15003, the producer of the hybrid peptide-polyketide antitumor drug bleomycin. *Chem. Biol.* 8, 725–738.
- (18) Studier, F. W. (2005) Protein production by auto-induction in high-density shaking cultures. *Protein Expression Purif.* 41, 207–234.
- (19) Otwinowski, Z., and Minor, W. (1997) Processing of X-ray diffraction data collected in oscillation mode. *Methods Enzymol.* 276, 306–315.
- (20) Adams, P. D., Grosse-Kunstleve, R. W., Hung, L. W., Ioerger, T. R., McCoy, A. J., Moriarty, N. W., Read, R. J., Sacchettini, J. C., Sauter, N. K., and Terwilliger, T. C. (2002) PHENIX: Building new software for automated crystallographic structure determination. *Acta Crystallogr. D* 58, 1948–1954.
- (21) Murshudov, G. N., Vagin, A. A., and Dodson, E. J. (1997) Refinement of macromolecular structures by the maximum-likelihood method. *Acta Crystallogr. D* 53, 240–255.
- (22) Potterton, E., Briggs, P., Turkenburg, M., and Dodson, E. (2003) A graphical user interface to the CCP4 program suite. *Acta Crystallogr. D* 59, 1131–1137.
- (23) Joosten, K., Cohen, S. X., Emsley, P., Mooij, W., Lamzin, V. S., and Perrakis, A. (2008) A knowledge-driven approach for crystallographic protein model completion. *Acta Crystallogr. D* 64, 416–424.
- (24) Emsley, P., and Cowtan, K. (2004) Coot: Model-building tools for molecular graphics. *Acta Crystallogr. D* 60, 2126–2132.
- (25) Dauter, Z. (2010) Carrying out an optimal experiment. *Acta Crystallogr. D* 66, 389–392.
- (26) Pidugu, L. S., Maity, K., Ramaswamy, K., Suroia, N., and Suguna, K. (2009) Analysis of proteins with the “hot dog” fold: Prediction of function and identification of catalytic residues of hypothetical proteins. *BMC Struct. Biol.* 9, 37.
- (27) Dillon, S. C., and Bateman, A. (2004) The hotdog fold: Wrapping up a superfamily of thioesterases and dehydratases. *BMC Bioinf.* 5, 109.
- (28) Krissinel, E., and Henrick, K. (2007) Inference of macromolecular assemblies from crystalline state. *J. Mol. Biol.* 372, 774–797.
- (29) Holm, L., Kääriäinen, S., Rosenström, P., and Schenkel, A. (2008) Searching protein structure databases with DALI-Lite v.3. *Bioinformatics* 24, 2780–2781.
- (30) Keatinge-Clay, A. (2008) Crystal structure of the erythromycin polyketide synthase dehydratase. *J. Mol. Biol.* 384, 941–953.
- (31) Akey, D. L., Razelun, J. R., Tehranisa, J., Sherman, D. H., Gerwick, W. H., and Smith, J. L. (2010) Crystal structures of dehydratase domains from the curacin polyketide biosynthetic pathway. *Structure* 18, 94–105.
- (32) Li, Y., Image, I. I., Xu, W., and Tang, Y. (2010) Classification, prediction, and verification of the regioselectivity of fungal polyketide synthase product template domains. *J. Biol. Chem.* 285, 22764–22773.
- (33) Crawford, J. M., Korman, T. P., Labonte, J. W., Vagstad, A. L., Hill, E. A., Kamari-Bidkorpheh, O., Tsai, S.-C., and Townsend, C. A. (2009) Structural basis for biosynthetic programming of fungal aromatic polyketide cyclization. *Nature* 461, 1139–1143.
- (34) Zhang, J., Van Lanen, S. G., Ju, J., Liu, W., Dorrestein, P. C., Li, W., Kelleher, N. L., and Shen, B. (2008) A phosphopantetheinylating polyketide synthase producing a linear polyene to initiate enediyne antitumor antibiotic biosynthesis. *Proc. Natl. Acad. Sci. U.S.A.* 105, 1460–1465.
- (35) Kotaka, M., Kong, R., Qureshi, I., Ho, Q. S., Sun, H., Liew, C. W., Goh, L. P., Cheung, P., Mu, Y., Lescar, J., and Liang, Z.-X. (2009) Structure and catalytic mechanism of the thioesterase CalE7 in enediyne biosynthesis. *J. Biol. Chem.* 284, 15739–15749.
- (36) Liew, C. W., Sharff, A., Kotaka, M., Kong, R., Sun, H., Qureshi, I., Bricogne, G., Liang, Z.-X., and Lescar, J. (2010) Induced-fit upon ligand binding revealed by crystal structures of the hot-dog fold thioesterase in dynemicin biosynthesis. *J. Mol. Biol.* 404, 291–306.
- (37) Keatinge-Clay, A. T., Shelat, A. A., Savage, D. F., Tsai, S.-C., Miercke, L. J. W., O’Connell, J. D., Khosla, C., and Stroud, R. M. (2003) Catalysis, specificity, and ACP docking site of *Streptomyces coelicolor* malonyl-CoA:ACP transacylase. *Structure* 11, 147–154.
- (38) Oefner, C., Schulz, H., D’Arcy, A., and Dale, G. E. (2006) Mapping the active site of *Escherichia coli* malonyl-CoA-acyl carrier protein transacylase (FabD) by protein crystallography. *Acta Crystallogr. D* 62, 613–618.
- (39) Tang, Y., Chen, A. Y., Kim, C., Cane, D. E., and Khosla, C. (2007) Structural and mechanistic analysis of protein interactions in module 3 of the 6-deoxyerythronolide B synthase. *Chem. Biol.* 14, 931–943.
- (40) Tang, Y., Kim, C., Mathews, I. I., Cane, D. E., and Khosla, C. (2006) The 2.7-Ångström crystal structure of a 194-kDa homodimeric fragment of the 6-deoxyerythronolide B synthase. *Proc. Natl. Acad. Sci. U.S.A.* 103, 11124–11129.
- (41) Ho, M.-C., Ménétret, J.-F., Tsuruta, H., and Allen, K. N. (2009) The origin of the electrostatic perturbation in acetoacetate decarboxylase. *Nature* 459, 393–397.
- (42) Benning, M. M., Haller, T., Gerlt, J. A., and Holden, H. M. (2000) New reactions in the crotonase superfamily: Structure of methylmalonyl CoA decarboxylase from *Escherichia coli*. *Biochemistry* 39, 4630–4639.
- (43) Pan, H., Tsai, S. C., Meadows, E. S., Miercke, L. J. W., Keatinge-Clay, A. T., O’Connell, J., Khosla, C., and Stroud, R. M. (2002) Crystal structure of the priming β -ketosynthase from the R1128 polyketide biosynthetic pathway. *Structure* 10, 1559–1568.
- (44) Dreier, J., and Khosla, C. (2000) Mechanistic analysis of a type II polyketide synthase. Role of conserved residues in the β -ketoacyl synthase-chain length factor heterodimer. *Biochemistry* 39, 2088–2095.
- (45) Bisang, C., Long, P. F., Cortés, J., Westcott, J., Crosby, J., Matharu, A. L., Cox, R. J., Simpson, T. J., Staunton, J., and Leadlay, P. F. (1999) A chain initiation factor common to both modular and aromatic polyketide synthases. *Nature* 401, 502–505.